Available online at www.sciencedirect.com

ScienceDirect

IFAC PapersOnline CONFERENCE PAPER ARCHIVE

IFAC PapersOnLine 51-29 (2018) 317–322

A Model-Based Speed and Course Controller for High-Speed ASVs

Bjørn-Olav H. Eriksen * **Morten Breivik** *

* *Centre for Autonomous Marine Operations and Systems*
Department of Engineering Cybernetics
Norwegian University of Science and Technology (NTNU)
NO-7491 Trondheim, Norway
E-mail: {bjorn-olav.h.eriksen, morten.breivik}@ieee.org

Abstract: Well-performing low-level vessel controllers are a necessity for marine motion control applications such as path following, trajectory tracking and collision avoidance for autonomous surface vehicles (ASVs). Designing such controllers are especially challenging for high-speed vessels operating in both the displacement, semi-displacement and planing regions. In this article, we build on a powerful framework for modeling, identification and control of high-speed ASVs in order to develop a model-based speed and course controller with high performance. The controller is shown to outperform a gain-scheduled proportional-integral feedback controller in full-scale experiments in the Trondheimsfjord, Norway. The controllers are compared both qualitatively and quantitatively using suitable performance metrics.

Keywords: Model-based control, autonomous surface vehicles, high-speed motion control

1. INTRODUCTION

Kinematic control applications such as path following and trajectory tracking (Fossen, 2011) rely on high-performance low-level vessel controllers. The same is the case for autonomy-enabling collision avoidance (COLAV) functionality (Kuwata et al., 2014; Eriksen and Breivik, 2017b; Eriksen et al., 2018). Hence, to be able to employ autonomous surface vehicles (ASVs) for a range of marine control applications, precise and robust low-level motion controllers are required.

In general, ASVs are small and agile vessels capable of operating at high speeds. Such vessels often operate in both the displacement, semi-displacement and planing regions. In the displacement region, the hydrostatic pressure mainly carries the vessel weight. When increasing the vessel speed, hydrodynamic effects will increase and eventually carry the majority of the vessel weight. When the hydrodynamic pressure dominates the hydrostatic pressure, the vessel operates in the planing region, and between the displacement and planing regions is the semi-displacement region (Fossen, 2011). Most modeling approaches assume that the vessel only operates in the displacement region, which makes modeling of high-speed ASVs challenging. This again makes it difficult to develop high-performance low-level motion controllers utilizing mathematical models of the vessel.

In (Breivik et al., 2008), an ASV speed and course controller using steady-state feedforward in speed is developed and used in full-scale trajectory tracking experiments with an ASV moving beyond the displacement region. The controller is extended with steady-state feedforward in yaw rate and used for formation control in (Breivik, 2010).

In this paper, we build upon a powerful approach for modeling, identification and control of high-speed ASVs operating in both the displacement, semi-displacement and planing regions (Eriksen and Breivik, 2017a). In particular, a vessel speed and yaw-rate controller employing model-based feedforward terms is developed in (Eriksen and Breivik, 2017a) and shown to outperform other controllers. Here, we extend this controller to also control the vessel course, which enables the vessel velocity to be controlled precisely. As such, it is important to note the difference between heading (yaw angle) and course, where the former relates to the direction which the vessel bow is pointing while the course is the direction which the vessel is traveling. When the vessel is maneuvering or under influence of external disturbances, the heading and course will in most cases not be aligned. The performance of the new model-based speed and course controller is evaluated through full-scale experiments in the Trondheimsfjord, Norway.

The rest of the paper is structured as follows: Section 2 presents the Telemetron ASV and gives a summary of the modeling and identification approach developed in (Eriksen and Breivik, 2017a). In Section 3, we develop the new speed and course controller, while Section 4 presents the results from the full-scale experiments. Finally, Section 5 concludes the paper and suggests some further work.

2. ASV PLATFORM AND MODELING

The vessel considered in this paper is the Maritime Robotics' Telemetron ASV, shown in Figure 1. This is a dual-use vessel, designed for both manned and unmanned operations. The vessel is 8.45 m long and capable of speeds up to 18 m/s. See Table 1 for more specifications.

2405-8963
Peer review under responsibility of International Federation of Automatic Control.
10.1016/j.ifacol.2018.09.504

Fig. 1. The dual-use Telemetron ASV, which is 8.45 m long and capable of speeds up to 18 m/s. Courtesy of Maritime Robotics.

Most ASVs are modeled using the well-known 3 degrees of freedom (DOF) model (Fossen, 2011):

$$\dot{\boldsymbol{\eta}} = \boldsymbol{R}(\psi)\boldsymbol{\nu} \tag{1a}$$

$$\boldsymbol{M}\dot{\boldsymbol{\nu}} + \boldsymbol{C}(\boldsymbol{\nu})\boldsymbol{\nu} + \boldsymbol{D}(\boldsymbol{\nu})\boldsymbol{\nu} = \boldsymbol{\tau} + \boldsymbol{\tau}_{\text{environment}}, \tag{1b}$$

where $\boldsymbol{\eta} = [N\ E\ \psi]^T$ is the vessel pose, $\boldsymbol{\nu} = [u\ v\ r]^T$ is the vessel body velocity, while $\boldsymbol{\tau}$ and $\boldsymbol{\tau}_{\text{environment}}$ are the control and environmental forces and moments, respectively. The matrix $\boldsymbol{R}(\psi)$ is a rotation matrix, while $\boldsymbol{M}$, $\boldsymbol{C}(\boldsymbol{\nu})$ and $\boldsymbol{D}(\boldsymbol{\nu})$ are the inertia, Coriolis/centripetal and damping matrices, respectively. Although the model (1) is frequently used for modeling vessels operating at high speeds, the model is developed under the assumption that the vessel operates in the displacement region. The operating region of a vessel can be approximated by computing the Froude number (Faltinsen, 2005). Using this number, it can be shown that an ASV with submerged length of 8 m exits the displacement region at around 3.54 m/s, while entering the planing region at approximately 8.86 m/s (Eriksen and Breivik, 2017a). Hence, an alternative model to (1) is required to develop a motion control system for a vessel like the Telemetron ASV.

2.1 Control-oriented modeling of high-speed ASVs

In (Eriksen and Breivik, 2017a), a data-driven control-oriented modeling approach for high-speed ASVs is proposed. Most ASVs are underactuated, making it impossible to independently control surge, sway and yaw simultaneously. One usually chooses to control the surge and yaw motion, leaving the sway motion uncontrolled. Therefore, a 2DOF model using the vessel speed over ground (SOG) $U = \sqrt{u^2 + v^2}$ and rate of turn (ROT) r as states is suitable for control purposes. The kinematics of the vessel using SOG and ROT can be described as:

$$\dot{\boldsymbol{\eta}} = \begin{bmatrix} \cos(\chi) & 0 \\ \sin(\chi) & 0 \\ 0 & 1 \end{bmatrix} \begin{bmatrix} U \\ r \end{bmatrix} \tag{2}$$

$$\dot{\chi} = r + \dot{\beta},$$

where r is the vessel ROT and $\chi = \psi + \beta$ is the vessel course with β being the vessel sideslip.

To model the vessel dynamics, we define a state vector $\boldsymbol{x} = [U\ r]^T$ and use a normalized 2DOF non-first principles model to model the vessel dynamics:

$$\boldsymbol{M}(\boldsymbol{x})\dot{\boldsymbol{x}} + \boldsymbol{\sigma}(\boldsymbol{x}) = \boldsymbol{\tau}, \tag{3}$$

Table 1. Telemetron ASV specifications.

Component	Description
Vessel hull	Polarcirkel Sport 845
Length	8.45 m
Width	2.71 m
Weight	1675 kg
Propulsion system	Yamaha 225 HP outboard engine
Motor control	Electro-mechanical actuation of throttle valve
Rudder control	Hydraulic actuation of outboard engine angle with proportional-derivate (PD) feedback control
Navigation system	Kongsberg Seatex Seapath 330+
Processing platform	Intel® i7 3.4 GHz CPU, running Ubuntu 16.04 Linux

where $\boldsymbol{M}(\boldsymbol{x}) = \text{diag}\,(m_U(\boldsymbol{x}), m_r(\boldsymbol{x}))$ is a diagonal state-dependent inertia matrix and $\boldsymbol{\sigma}(\boldsymbol{x}) = [\sigma_U(\boldsymbol{x})\ \sigma_r(\boldsymbol{x})]^T$ is a vector of damping terms, both being nonlinear in terms of the state vector $\boldsymbol{x}$. The vector $\boldsymbol{\tau} = [\tau_m\ \tau_\delta]^T$ is a normalized control input, where $\tau_m \in [0, 1]$ and $\tau_\delta \in [-1, 1]$ are the motor throttle and rudder control input, respectively.

The terms of the inertia matrix $\boldsymbol{M}(\boldsymbol{x})$ and damping term $\boldsymbol{\sigma}(\boldsymbol{x})$ are defined using high-order polynomial functions:

$$\begin{aligned} m_U(\boldsymbol{x}) &= \boldsymbol{\phi}_m(\boldsymbol{x})^T\boldsymbol{\beta}_{m_U}, \quad \sigma_U(\boldsymbol{x}) = \boldsymbol{\phi}_\sigma(\boldsymbol{x})^T\boldsymbol{\beta}_{\sigma_U} \\ m_r(\boldsymbol{x}) &= \boldsymbol{\phi}_m(\boldsymbol{x})^T\boldsymbol{\beta}_{m_r}, \quad \sigma_r(\boldsymbol{x}) = \boldsymbol{\phi}_\sigma(\boldsymbol{x})^T\boldsymbol{\beta}_{\sigma_r}, \end{aligned} \tag{4}$$

where $\boldsymbol{\phi}_m(\boldsymbol{x})$ and $\boldsymbol{\phi}_\sigma(\boldsymbol{x})$ are vectors of basis functions, called regressors, while $\boldsymbol{\beta}_{m_U}, \boldsymbol{\beta}_{m_r}, \boldsymbol{\beta}_{\sigma_U}$ and $\boldsymbol{\beta}_{\sigma_r}$ are parameter vectors. Notice that the terms are linear in the parameters, which allows the use of linear regression (Bishop, 2006) to find the optimal parameter vectors. The regressors are defined as a fourth-order polynomial function for the damping:

$$\begin{aligned} \boldsymbol{\phi}_\sigma(\boldsymbol{x}) = \big[&1,\ U,\ r,\ U^2,\ Ur,\ r^2,\ U^3,\ U^2r,\ Ur^2, \\ &r^3,\ U^4,\ U^3r,\ U^2r^2,\ Ur^3,\ r^4\big]^T, \end{aligned} \tag{5}$$

and as the same fourth-order polynomial plus an asymptotic function for the inertia:

$$\begin{aligned} \boldsymbol{\phi}_M(\boldsymbol{x}) = \big[&1,\ U,\ r,\ U^2,\ Ur,\ r^2,\ U^3, \\ &U^2r,\ Ur^2,\ r^3,\ U^4,\ U^3r, \\ &U^2r^2,\ Ur^3,\ r^4,\ \tanh(a(U-b))\big]^T, \end{aligned} \tag{6}$$

where a and b are parameters controlling the asymptotic term. The order of the polynomials is chosen sufficiently high to capture hydrodynamic damping and actuator dynamics. The asymptotic term in the inertia regressor is motivated by experiments showing a large decrease in the inertia for increasing SOG at low speeds.

2.2 Parameter identification

As mentioned, the linearity of parameters in the terms (4) allows for the use of linear regression to identify optimal parameter values. For a model on the form:

$$y = \boldsymbol{\phi}(\boldsymbol{x})^T\boldsymbol{\beta}, \tag{7}$$

one can, given a set of N data points $\{\boldsymbol{x}_1, \boldsymbol{x}_2, \ldots, \boldsymbol{x}_N\}$ and $\{y_1, y_2, \ldots, y_N\}$, define a weighted square loss function:

$$\epsilon = \frac{1}{N}\sum_{i=1}^{N} W_{ii}\left(y_i - \boldsymbol{\phi}(\boldsymbol{x}_i)^T\hat{\boldsymbol{\beta}}\right)^2, \tag{8}$$

with $\hat{\boldsymbol{\beta}}$ being an estimate of the true parameter vector $\boldsymbol{\beta}$, and W_{ii} being a weight on data point i. Defining $\boldsymbol{Y} = [y_1\ y_2\ \dots\ y_N]^T$, $\boldsymbol{X} = [\boldsymbol{\phi}(\boldsymbol{x}_1)\ \boldsymbol{\phi}(\boldsymbol{x}_2)\ \dots\ \boldsymbol{\phi}(\boldsymbol{x}_N)]^T$ and $\boldsymbol{W} = \text{diag}\,(W_{11}, W_{22}, \dots, W_{NN})$, we can find the parameter vector $\hat{\boldsymbol{\beta}}$ which minimizes (8) using linear regression as:

$$\hat{\boldsymbol{\beta}} = (\boldsymbol{X}^T\boldsymbol{W}\boldsymbol{X})^{-1}\boldsymbol{X}^T\boldsymbol{W}\boldsymbol{Y}. \tag{9}$$

A well-known problem with linear regression is the problem of overfitting. To reduce this problem, one can introduce regularization, which penalizes parameter vectors with large parameter values (Bishop, 2006). The loss function (8) is then reformulated as:

$$\epsilon = \frac{1}{N}\sum_{i=1}^{N} W_{ii}\left(y_i - \boldsymbol{\phi}(\boldsymbol{x}_i)^T\hat{\boldsymbol{\beta}}\right)^2 + \lambda R(\hat{\boldsymbol{\beta}}), \tag{10}$$

where $\lambda > 0$ is a regularization parameter and $R(\hat{\boldsymbol{\beta}})$ is a regularization function. In (Eriksen and Breivik, 2017a), ℓ_1 regularization is used, since it favors sparse parameter vectors. Hence, the regularization function is defined as $R(\hat{\boldsymbol{\beta}}) = \left\|\hat{\boldsymbol{\beta}}\right\|_1$.

In (Eriksen and Breivik, 2017a), a number of vessel experiments were conducted in order to obtain measurements of the vessel inertia and damping. These experiments were based on series of step responses in the motor throttle τ_m and rudder angle τ_δ. Based on the experiments, three datasets of measurements were obtained:

$$\mathcal{D}_{\boldsymbol{\sigma}} = \{\{\boldsymbol{x}_1, \boldsymbol{x}_2, \dots, \boldsymbol{x}_{N_\sigma}\}, \{\boldsymbol{\sigma}_1, \boldsymbol{\sigma}_2, \dots, \boldsymbol{\sigma}_{N_\sigma}\}\}, \tag{11}$$

$$\mathcal{D}_{m_U} = \Big\{\{\boldsymbol{x}_1, \boldsymbol{x}_2, \dots, \boldsymbol{x}_{N_{m_U}}\}, \{m_{U_1}, m_{U_2}, \dots, m_{U_{N_{m_U}}}\}\Big\}, \tag{12}$$

$$\mathcal{D}_{m_r} = \Big\{\{\boldsymbol{x}_1, \boldsymbol{x}_2, \dots, \boldsymbol{x}_{N_{m_r}}\}, \{m_{r_1}, m_{r_2}, \dots, m_{r_{N_{m_r}}}\}\Big\}. \tag{13}$$

The set $\mathcal{D}_{\boldsymbol{\sigma}}$ contains vessel states and damping measurements, $\mathcal{D}_{m_U}$ contains vessel states and measurements of SOG inertia while $\mathcal{D}_{m_r}$ contains vessel states and measurements of ROT inertia. Using the data in (11)–(13), the parameter vectors $\boldsymbol{\beta}_{m_U}, \boldsymbol{\beta}_{m_r}, \boldsymbol{\beta}_{\sigma_U}$ and $\boldsymbol{\beta}_{\sigma_r}$ in (4) are identified using linear regression with ℓ_1 regularization. Figures 2 and 3 show the resulting model terms.

Figure 4 shows a comparison between real and simulated vessel responses for the same control input sequence. The real vessel response in Figure 4 was not used in the identification process, hence the comparison can be used to qualitatively verify the identified model. There are some deviations between the real and simulated responses, but the model is considered accurate enough for control purposes.

Interested readers are referred to (Eriksen and Breivik, 2017a) for more details on the modeling and identification framework.

3. ASV SPEED AND COURSE CONTROLLER

In (Eriksen and Breivik, 2017a), the model (3) is used for control of the vessel SOG and ROT using model-based

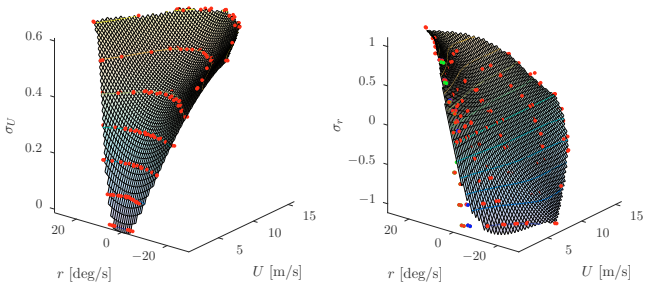

(a) (b)

Fig. 2. Surface plot of the damping term $\boldsymbol{\sigma}(\boldsymbol{x})$. The scatter points are the data points in $\mathcal{D}_{\boldsymbol{\sigma}}$ where red, blue and green points have weights $W = 1$, $W = 0.5$ and $W = 0.1$, respectively (Eriksen and Breivik, 2017a).

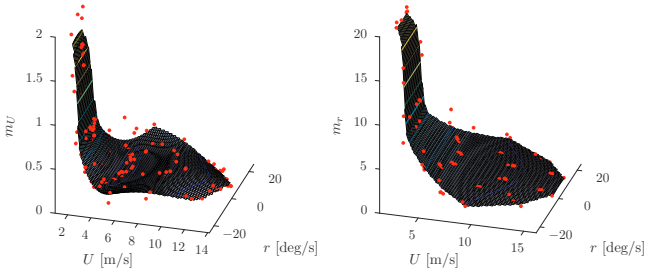

(a) (b)

Fig. 3. Surface plot of the inertia terms in $\boldsymbol{M}(\boldsymbol{x})$. The scatter points are the data points in $\mathcal{D}_{m_U}$ and $\mathcal{D}_{m_r}$ (Eriksen and Breivik, 2017a).

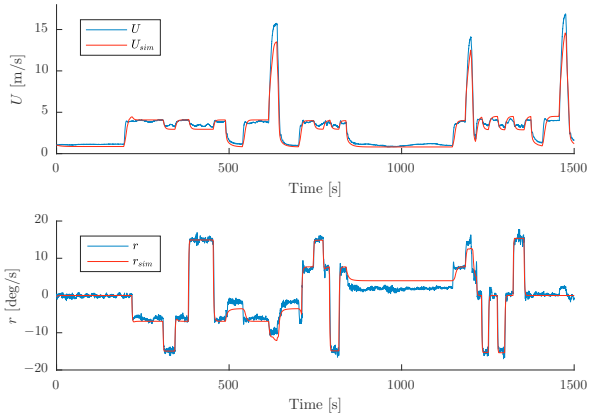

Fig. 4. Comparison of real and simulated vessel responses. The deviation at high SOG is caused by leaving the valid domain of the identified model (Eriksen and Breivik, 2017a).

feedforward terms. A controller named the feedforward feedback (FF-FB) controller is suggested as:

$$\boldsymbol{\tau}_{\text{FF-FB}} = \boldsymbol{M}(\boldsymbol{x})\dot{\boldsymbol{x}}_d + \boldsymbol{\sigma}(\boldsymbol{x}_d) - \boldsymbol{M}(\boldsymbol{x})\boldsymbol{K}_p\tilde{\boldsymbol{x}} - \boldsymbol{K}_i\int_{t_0}^{t}\tilde{\boldsymbol{x}}(\gamma)\mathrm{d}\gamma, \tag{14}$$

where $\boldsymbol{x}_d = [U_d\ r_d]^T$ is a vector of desired SOG and ROT, $\tilde{\boldsymbol{x}} = \boldsymbol{x} - \boldsymbol{x}_d$ is the control error, $\boldsymbol{K}_p > 0$ is

a diagonal proportional gain matrix and $\boldsymbol{K}_i > 0$ is a diagonal integral gain matrix. The controller (14) is shown to have significantly better performance than a gain-scheduled proportional-integral (PI) feedback controller, a pure feedforward controller and a feedback-linearizing controller.

In many applications, it is desirable to control the vessel kinematics, for instance by controlling the ASV course. Similar to the design of vessel SOG and ROT controllers in (Eriksen and Breivik, 2017a), utilizing model-based feedforward terms should increase the closed-loop performance of a controller also for the vessel kinematics. Hence, we propose to extend the FF-FB controller (14) with feedback terms for the vessel course χ, defining the feedforward-feedback course (FF-FB-C) controller as:

$$\begin{aligned}\boldsymbol{\tau}_{\text{FF-FB-C}} &= \boldsymbol{M}(\boldsymbol{x})\dot{\boldsymbol{x}}_d + \boldsymbol{\sigma}(\boldsymbol{x}_d) \\ &\quad - \boldsymbol{M}(\boldsymbol{x})\bar{\boldsymbol{K}}_p\tilde{\boldsymbol{\zeta}} - \bar{\boldsymbol{K}}_i\int_{t_0}^{t}\tilde{\boldsymbol{\zeta}}_1(\gamma)\mathrm{d}\gamma, \quad (15)\end{aligned}$$

where $\tilde{\boldsymbol{\zeta}}$ and $\tilde{\boldsymbol{\zeta}}_1$ are the error terms:

$$\begin{aligned}\tilde{\boldsymbol{\zeta}} &= \begin{bmatrix}\boldsymbol{x}-\boldsymbol{x}_d \\ \Upsilon(\chi-\chi_d)\end{bmatrix} = \begin{bmatrix}\tilde{U} \\ \tilde{r} \\ \tilde{\chi}\end{bmatrix} \\ \tilde{\boldsymbol{\zeta}}_1 &= \begin{bmatrix}\tilde{U} \\ \tilde{\chi}\end{bmatrix},\end{aligned} \quad (16)$$

with χ_d being the desired vessel course and $\Upsilon : \mathbb{R} \to S^1$ mapping an angle to the domain $[-\pi, \pi)$. The matrices $\bar{\boldsymbol{K}}_p$ and $\bar{\boldsymbol{K}}_i$ contain positive proportional and integral gains, respectively:

$$\begin{aligned}\bar{\boldsymbol{K}}_p &= \begin{bmatrix}k_{p_U} & 0 & 0 \\ 0 & k_{p_r} & k_{p_\chi}\end{bmatrix} \\ \bar{\boldsymbol{K}}_i &= \begin{bmatrix}k_{i_U} & 0 \\ 0 & k_{i_\chi}\end{bmatrix}.\end{aligned} \quad (17)$$

Through (2), the relationship between the course and ROT is stated as $r = \dot{\chi} - \dot{\beta}$, where the sideslip β enters the equation. Currently, we do not have a sideslip model of the Telemetron ASV. However, we have seen in experiments that at moderate speeds the sideslip is sufficiently constant such that $\dot{\beta} \approx 0$ can be assumed without major implications. We therefore simplify the relation by assuming constant sideslip and defining the desired ROT as:

$$\begin{aligned}r_d &= \dot{\chi}_d \\ \dot{r}_d &= \ddot{\chi}_d.\end{aligned} \quad (18)$$

Hence, assuming a constant or slowly-varying sideslip, the controller (15) is a speed and course controller which is able to precisely control the vessel velocity, which is required for kinematic control applications.

4. EXPERIMENTAL RESULTS

The controller performance is tested through full-scale experiments in the Trondheimsfjord in Norway on the 10th of October 2017 using the Telemetron ASV. The sea state was considered as slight, which refers to significant wave heights of 0.5–1.25 m (Prince and Bishop, 1974).

The FF-FB-C controller is compared to a PI feedback controller with gain scheduling:

$$\boldsymbol{\tau}_{\text{FB-C}} = -\boldsymbol{M}(\boldsymbol{x})\bar{\boldsymbol{K}}_p\tilde{\boldsymbol{\zeta}} - \bar{\boldsymbol{K}}_i\int_{t_0}^{t}\tilde{\boldsymbol{\zeta}}_1(\gamma)\mathrm{d}\gamma, \quad (19)$$

which is named the feedback course (FB-C) controller. Notice that the FB-C controller is obtained by removing the feedforward terms of (15). The same controller parameters were used for both controllers:

$$\begin{aligned}k_{p_U} &= 0.6 \quad & k_{i_U} &= 0.01 \\ k_{p_\chi} &= 0.15 \quad & k_{i_\chi} &= 0.015 \\ k_{p_r} &= 0.35. & & \end{aligned} \quad (20)$$

To generate the derivatives required for the controllers, the desired SOG trajectory $U_d(t)$ must be continuously differentiable, while the desired course trajectory $\chi_d(t)$ must be twice continuously differentiable. To ensure this, a second order reference filter is used to generate $U_d(t)$, while a third order reference filter is used to generate $\chi_d(t)$.

4.1 Performance metrics

To quantitatively evaluate the performance of the controllers, performance metrics are useful. For simplicity in analyzing the performance, we wish to combine both speed and course errors in the metrics. Since these have different units, we must introduce some sort of weighted sum (Eriksen and Breivik, 2017a). To do this, we define the normalized signals $\bar{U}, \bar{U}_d, \bar{\chi}, \bar{\chi}_d \in [0, 1]$ for the expected operational space of the vessel. For the Telemetron ASV, the expected operating space is up to 18 m/s for SOG, and 2π rad for course since it resides in S^1. We then define a combined error term and control input as:

$$\bar{e}(t) = \left\| \begin{bmatrix}\bar{U}(t) - \bar{U}_d(t) \\ \bar{\chi}(t) - \bar{\chi}_d(t)\end{bmatrix} \right\|_2 \quad (21)$$

and

$$\bar{\tau}(t) = \|\boldsymbol{\tau}\|_2. \quad (22)$$

Different performance metrics are used to evaluate different qualities. The integral of absolute error (IAE) penalizes deviation from the desired speed and course:

$$IAE(t) = \int_{t_0}^{t}\bar{e}(\gamma)\mathrm{d}\gamma, \quad (23)$$

and serves as a measure of control precision. The integral of absolute differentiated control (IADC) has previously been used as a part of a combined performance metric in (Sørensen et al., 2016):

$$IADC(t) = \int_{t_0}^{t}|\dot{\bar{\tau}}(\gamma)|\mathrm{d}\gamma, \quad (24)$$

and serves as a measure of wear and tear on the actuators. The integral of absolute error times the integral of absolute differentiated control (IAE-ADC) combines IAE and IADC, and is computed as:

$$IAE\text{-}ADC(t) = \int_{t_0}^{t}\bar{e}(\gamma)\mathrm{d}\gamma\int_{t_0}^{t}|\dot{\bar{\tau}}(\gamma)|\mathrm{d}\gamma, \quad (25)$$

and is a measure of control precision scaled by wear and tear (Eriksen and Breivik, 2017a). Finally, the integral of absolute error times work (IAEW) scales IAE with the energy consumption (Sørensen and Breivik, 2015), and is computed as:

$$IAEW(t) = \int_{t_0}^{t}\bar{e}(\gamma)\mathrm{d}\gamma\int_{t_0}^{t}P(\gamma)\mathrm{d}\gamma, \quad (26)$$

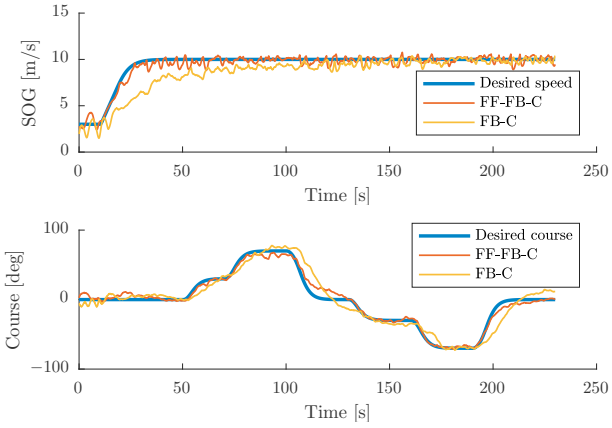

Fig. 5. Test 1: High-speed trajectory with constant SOG and steps and steady states in course.

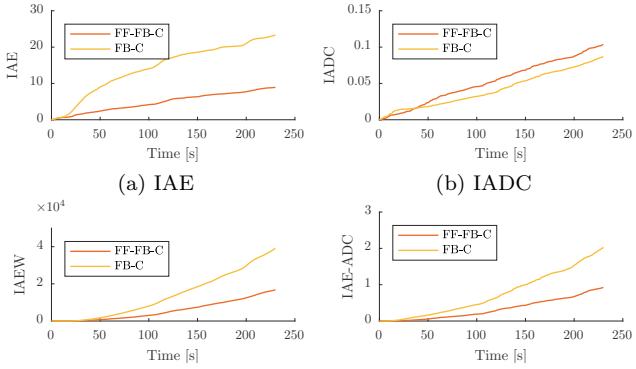

(a) IAE (b) IADC

(c) IAEW (d) IAE-ADC

Fig. 6. Performance metrics for Test 1. The FF-FB-C controller clearly outperforms the FB-C controller on all metrics except the IADC.

where $P(t)$ is the mechanical power applied by the vessel motor. Hence, IAEW serves as a measure of the energy efficiency. In this work, we approximate the mechanical power as linear with the motor throttle, hence $P \propto \tau_m$.

4.2 Full-scale experiments

In this section, we present experimental results from two test scenarios:

- Test 1: A high-speed trajectory with constant SOG and step changes in course, with steady states in between.
- Test 2: A high-speed trajectory with step changes and steady states in both SOG and course.

Test 1 For the first test, we have a high-speed trajectory with constant SOG, while attempting to follow a course trajectory consisting of both steps and steady states. The resulting trajectories are shown in Figure 5. It is clear that the FF-FB-C controller follows the desired SOG trajectory better than the FB-C controller, which also is the case for the course. In particular, the FF-FB-C controller has a better transient response. The FB-C controller struggles to follow a changing reference, while also having problems with overshoots, which is a natural result of using integral terms to stabilize the controlled variables.

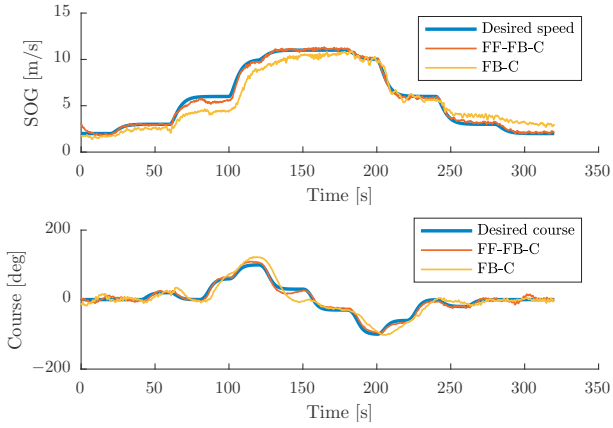

Fig. 7. Test 2: High-speed trajectory with steps and steady states in both SOG and course.

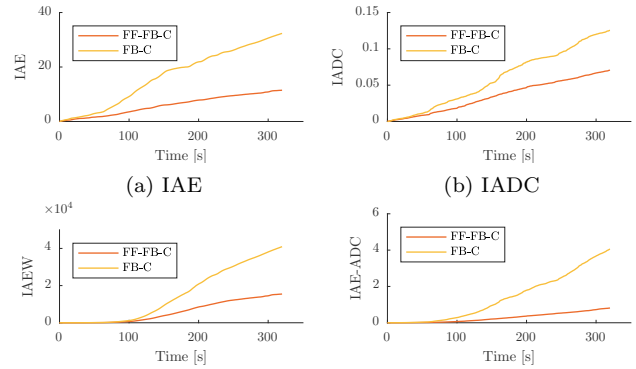

(a) IAE (b) IADC

(c) IAEW (d) IAE-ADC

Fig. 8. Performance metrics for Test 2. The FF-FB-C controller clearly outperforms the FB-C controller on all the metrics.

From the performance metrics in Figure 6, we see that the FF-FB-C controller has the best performance. In particular, the IAE is much lower with the FF-FB-C controller than the FB-C controller. The control usage (IADC) is slightly higher for the FF-FB-C controller, but when scaled with the control performance (IAE-ADC), the FF-FB-C outperforms the FB-C controller. Also, the energy efficiency (IAEW) is much better with the FF-FB-C controller than with the FB-C controller.

Test 2 The second test consists of steps and steady states in both SOG and course, testing the performance both at relatively low and high speeds. The trajectories are shown in Figure 7, while the performance metrics are shown i Figure 8. Again, it is clear that the FF-FB-C controller has much better transient response than the FB-C controller, both in SOG and course. The FF-FB-C controller also has the best steady-state performance. In this scenario, all the performance metrics are in favor of the FF-FB-C controller. Notice in particular the control precision (IAE) and energy efficiency (IAEW) which are 2–3 times better with the FF-FB-C controller than with the FB-C controller.

The performance metrics for both tests are summarized in Table 2.

Table 2. Performance metrics for both controllers in both tests. The controller with the best performance for each metric in each test is highlighted in bold.

Test case	Controller	IAE	IADC	IAE-ADC	IAEW
Test 1	FF-FB-C	**8.9**	$1.4 \cdot 10^{-1}$	**1.3**	$\mathbf{1.7 \cdot 10^{4}}$
	FB-C	$2.3 \cdot 10^{1}$	$\mathbf{1.2 \cdot 10^{-1}}$	2.8	$3.9 \cdot 10^{4}$
Test 2	FF-FB-C	$\mathbf{1.1 \cdot 10^{1}}$	$\mathbf{7.1 \cdot 10^{-2}}$	$\mathbf{8.1 \cdot 10^{-1}}$	$\mathbf{1.5 \cdot 10^{4}}$
	FB-C	$3.2 \cdot 10^{1}$	$1.3 \cdot 10^{-1}$	4.1	$4.1 \cdot 10^{4}$

5. CONCLUSION AND FURTHER WORK

We have proposed a SOG and course controller for high-speed ASVs operating in the displacement, semi-displacement and planing regions. The controller employs model-based feedforward terms, based on the FF-FB velocity controller developed in (Eriksen and Breivik, 2017a). Through full-scale experiments in the Trondheimsford, Norway, the controller is compared to a PI feedback controller with gain scheduling. From the experiments, it is clear that using model-based feedforward terms in combination with feedback terms greatly improve the control performance compared to using a pure feedback controller. The performance is particularly improved for time-varying references.

The proposed speed and course controller has subsequently been successfully used for full-scale closed-loop COLAV experiments during the autumn of 2017 (Eriksen and Breivik, 2018). In future work, we would also like to use the proposed controller for other kinematic control applications, such as for example path following and trajectory tracking.

ACKNOWLEDGEMENTS

This work was supported by the Research Council of Norway through project number 244116 and the Centres of Excellence funding scheme with project number 223254. The authors would like to express great gratitude to Kongsberg Maritime and Maritime Robotics for providing high-grade navigation technology and the Telemetron ASV at our disposal for the experiments.

REFERENCES

Bishop, C.M. (2006). *Pattern Recognition and Machine Learning*. Springer Science + Business Media.

Breivik, M. (2010). *Topics in Guided Motion Control of Marine Vehicles*. Ph.D. thesis, Norwegian University og Science and Technology (NTNU), Trondheim, Norway.

Breivik, M., Hovstein, V.E., and Fossen, T.I. (2008). Straight-line target tracking for unmanned surface vehicles. *Modeling, Identification and Control*, 29(4), 131–149.

Eriksen, B.-O.H. and Breivik, M. (2017a). *Modeling, Identification and Control of High-Speed ASVs: Theory and Experiments*, 407–431. Springer International Publishing, Cham.

Eriksen, B.-O.H. and Breivik, M. (2017b). MPC-based mid-level collision avoidance for ASVs using nonlinear programming. In *Proc. of IEEE CCTA*. Kohala Coast, Hawai'i, USA.

Eriksen, B.-O.H. and Breivik, M. (2018). The branching course MPC algorithm for maritime collision avoidance. *Journal of Field Robotics - To be submitted*.

Eriksen, B.-O.H., Wilthil, E.F., Flåten, A.L., Brekke, E.F., and Breivik, M. (2018). Radar-based maritime collision avoidance using dynamic window. In *Proc. of IEEE Aerospace*. Big Sky, MT, USA.

Faltinsen, O.M. (2005). *Hydrodynamics of High-Speed Marine Vehicles*. Cambridge University Press.

Fossen, T.I. (2011). *Handbook of Marine Craft Hydrodynamics and Motion Control*. John Wiley & Sons Ltd.

Kuwata, Y., Wolf, M.T., Zarzhitsky, D., and Huntsberger, T.L. (2014). Safe maritime autonomous navigation with COLREGS, using velocity obstacles. *IEEE J. Oceanic Eng.*, 39(1), 110–119.

Prince, W.G. and Bishop, R.E.D. (1974). *Probabilistic Theory of Ship Dynamics*. Chapman and Hall.

Sørensen, M.E.N., Bjørne, E.S., and Breivik, M. (2016). Performance comparison of backstepping-based adaptive controllers for marine surface vessels. In *Proc. of IEEE CCA*. Buenos Aires, Argentina.

Sørensen, M.E.N. and Breivik, M. (2015). Comparing nonlinear adaptive motion controllers for marine surface vessels. In *Proc. of the 10th IFAC MCMC*. Copenhagen, Denmark.